Biochimica et Biophysica Acta, 554 (1979) 479—497

BBA 78408

VOLTAGE-INDUCED CONDUCTANCE IN HUMAN ERYTHROCYTE MEMBRANES

KAZUHIKO KINOSITA *, Jr. and TIAN YOW TSONG **

Department of Physiological Chemistry, The Johns Hopkins University School of Medicine, Baltimore, MD 21205 (U.S.A.)

(Received September 20th, 1978)
(Revised manuscript received February 6th, 1979)

Key words: Membrane conductance; Pore; Ion permeability; (Human erythrocyte membrane)

Summary

Isotonic suspensions of erythrocytes were exposed to intense electric fields for a duration in microseconds. Time-dependent increase in the conductivity of the suspension was observed under fields greater than a threshold of about 1.5 kV/cm. The threshold was independent of the ionic strength of the medium, and changed little with temperature or with the rise time of the applied field. Under fields greater than 3 kV/cm, the time course of the conductivity increase consisted of a rapid (approx. 1 μs) and a slow (approx. 100 μs) phases. The increase is attributed primarily to large membrane conductance induced by the applied field. The membrane conductance is in the order of 10 Ω^{-1}/cm^2 in the rapid phase and 10^2 Ω^{-1}/cm^2 in the slow phase. Comparison with previous results indicates that this induced membrane conductance corresponds to the formation of aqueous pores in the cell membrane. After the applied field was removed, the conductivity of the suspension returned nearly to its initial value, indicating that the induced membrane conductance is strongly dependent on the membrane potential. The conductivity then increased again in the time range of 10 s. This is attributed to the diffusional efflux of intracellular ions through the voltage-induced pores. From the rate of the efflux, number of the pores/cell is estimated to be in the order of 10^2. Final stage of the conductivity change was a slow decrease, corresponding to the colloid osmotic swelling of the perforated cells.

* Present address: The Institute of Physical and Chemical Research, Hirosawa, Wako-shi, Saitama 351, Japan.
** To whom correspondence should be addressed.
Abbreviation: ANS, 1-anilino-8-naphthalene sulfonate.

Introduction

It has been known that exposure of a cell suspension to an electric pulse of intensity in the range of kV/cm and of duration in μseconds results in a dramatic increase of the permeability of the cell membranes and, in many cases, in the lysis of the cells [1—5]. The effect has been attributed to a large transmembrane potential induced by the externally applied field [1,3,6]. Basic mechanism of this voltage-induced permeability change appears to be common to many cellular systems [7], and has been extensively studied for erythrocytes [3—8].

In human erythrocytes, a transmembrane potential exceeding a critical value of 1 V, which corresponds to an applied field intensity of 2.2 kV/cm, opens up aqueous pores in the cell membranes [6—8]. The effective diameter of the pores is about 1 nm and can be varied by the adjustment of the field intensity, field duration, and the ionic strength of the suspending medium [7,8]. Permeation of small ions or molecules through these pores and the accompanying water influx due to the colloid osmotic pressure of hemoglobin lead to gradual swelling and eventual lysis of the erythrocytes [6,7]. The pores remain open for many hours at low temperatures but are annealed completely on incubation at 37°C. In a proper medium, resealing of the perforated cells is achieved without causing hemolysis; the resealed erythrocytes appear to be intact in many respects [8].

Introduction of the pores of a desired size in cell membranes by this voltage-pulsation technique followed by the resealing will enable the preparation of apparently intact cells with altered intracellular compositions. Loading of erythrocytes with foreign molecules, for example, has already been demonstrated [8]; when the loaded erythrocytes were returned into the circulation, they survived with a normal lifetime and retained the entrapped molecules [9]. Thus, the technique is potentially a very useful tool in clinical applications such as drug delivery as well as in basic researches concerning transport phenomena, intracellular metabolism, control of intracellular activities by small ligand molecules, etc.

In addition to these possible applications, clarification of the mechanism of the voltage-induced pore formation may provide information on the porocity, structures and functions of biological membranes. Previous studies have suggested a two step mechanism [6,7] for the pore formation, where the initial perforation in response to a suprathreshold potential is followed by time-dependent expansion of the pore size, the latter process being facilitated by higher field intensities and/or lower ionic strengths. Molecular events underlying this phenomenological description, however, are not yet clear.

Here we have investigated the kinetics of the pore formation in human erythrocyte membranes by conductivity measurements. When a weak electric field is applied to a suspension of erythrocytes, current bypasses the cells because of the high resistivity of the cell membranes compared to that of the medium [10]. In a sufficiently strong field, the membranes will be perforated with the pores, through which current will penetrate the cell interior. Thus the process of pore formation will be detected as an increase in the conductivity of the cell suspension.

Materials and Methods

Fresh human blood was obtained from healthy young adults by venipuncture in the presence of heparin. Erythrocytes were washed three times by centrifugation at $1000 \times g$ for 10 min at 4°C with a solution containing 150 mM NaCl and 7 mM sodium phosphate buffer, pH 7.0; buffy coats were carefully removed. Packed cells were then resuspended in a mixture of the above NaCl solution and a 272 mM sucrose solution (both were assumed to be isotonic) and kept at 0—4°C until just prior to the pulsation; volume concentration (hematocrit) of the final suspension was adjusted to 19% (corrected for the trapped extracellular fluid estimated as [^{14}C]sucrose accessible space). Hereafter, the composition of a suspending medium will be denoted by the volume ratio of the isotonic saline and the sucrose solution.

A voltage-pulsation device previously described [6] has been modified as shown in Fig. 1. Major modifications are the followings: (i) in order to eliminate the effect of polarization at the surfaces of the electrodes, they were covered with platinized platinum [11]. (ii) Temperature of the sample was controlled by circulating distilled water inside the electrodes. (iii) A trigger-pulse generator external to the Cober high voltage pulser enabled the application of two successive pulses of different durations with a controlled interval. (iv) Current increment during pulsation rather than total current was measured by a differential circuit.

In the present study, conductivity, κ, of a sample is defined by

$$\kappa = (I/V)(d/A) \tag{1}$$

where I and V are the magnitude of total current and applied voltage, respectively, and d and A are the thickness and the cross-section of the sample. The change in κ during and after high voltage pulsation was estimated from I and V values obtained in the following five types of measurements. (a) In all experiments, the initial conductivity, κ_0, or the conductivity of the untreated sample, was first measured under a sinusoidal voltage of frequency at 1 kHz. The pulsation cell was placed between the pair of clamps shown below the electrodes in Fig. 1, and the sine-wave generator was set at a peak-to-peak voltage of 0.2 V for high ionic media (e.g. isotonic NaCl) or 2 V for low ionic media (e.g. 10% NaCl/90% sucrose isotonic mixture). Then, 20 μl of a cold erythrocyte suspension was introduced into the central cavity between the electrodes, and the magnitude of the current was recorded against time. The current reached a steady-state value within several seconds, indicating rapid equilibration of temperature. The initial conductivity, κ_0, was calculated from Eqn. 1, where the cell constant, d/A, was determined by the same type of masurement on 0.1 M KCl (the cell constant estimated from the volume and the thickness of the sample was greater by about 5%, indicating a small meniscus effect). In some cases, κ_0 was also determined at higher frequencies up to 30 kHz; there was not frequency dependence.

(b) Conductivity increment, $\Delta\kappa \equiv \kappa - \kappa_0$, during high voltage pulsation was measured as follows: after the determination of κ_0 in (a), the pulsation cell containing the sample was transferred onto the upper pair of clamps in Fig. 1. When the high voltage pulser delivered a square-wave pulse, the oscilloscopes 1

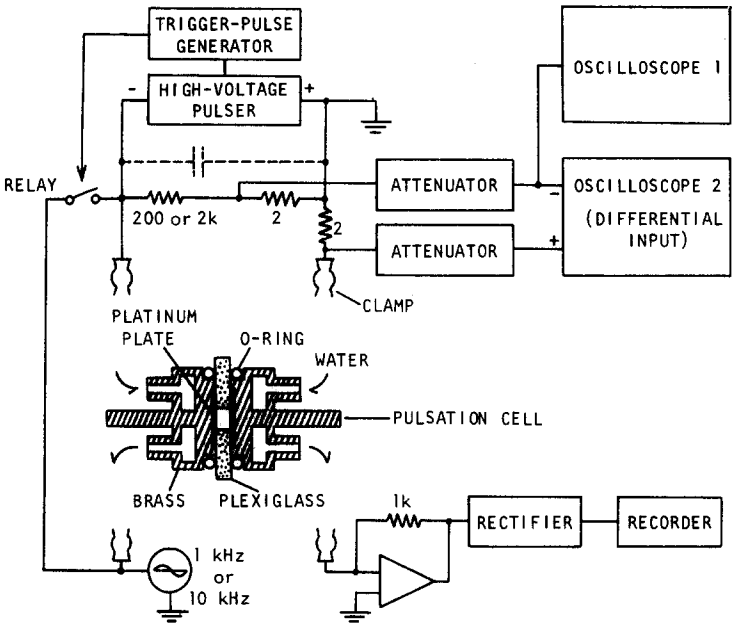

Fig. 1. A schematic diagram of the voltage-pulsation device and the measuring circuits. The pulsation cell consists of a pair of cylindrical brass electrodes with an internal cavity for temperature control, and a plexiglass spacer of 2 mm thickness having a central hole with a diameter of 3 mm and a narrow V-shaped slit connecting the central hole and the edge. The surface of the electrodes opposing the spacer is covered with a platinized platinum disk. The two electrodes are firmly pressed against the spacer by a plexiglass holder not shown in the figure, and held by the upper or the lower pair of metal clamps through which voltage is applied. A sample suspension is introduced into the central cylindrical cavity through the V-shaped slit. A trigger-pulse generator delivers either a single or double square-wave pulses, which are amplified by a Cober 605P high voltage pulser and fed to the sample. Insertion of a shunt capacitance shown (------) enables the application of linearly increasing voltage. Voltage and current signals are picked up by the 2-ohm resistors, attenuated by resistive T circuits, and fed to a differential unit (7A22) of a Tektronix 7704A oscilloscope. Voltage signal can be monitored by a separate oscilloscope (Tektronix 5301N storage-scope with 5A22N vertical unit) or by a second vertical unit of the 7704A in the dual trace mode. The circuit shown at the bottom is used for the measurement of slow conductivity changes. A sinusoidal voltage is applied to the electrodes, and the resultant sinusoidal current is converted to voltage signal by the 1 kohm resistor, rectified, and recorded on a chart recorder.

and 2 displayed a_1V and $a_2I - a_1V$, respectively, where a_1 and a_2 are the attenuation ratios determined by the two attenuators. First, a_1 and a_2 were so adjusted as to nullify the signal at oscilloscope 2 under a 100 V pulse, which corresponded to a field intensity, E ($=V/d$), of 0.5 kV/cm. Under this condition, a_1/a_2 gave I/V, with which κ was estimated from Eqn. 1; the result was always in agreement with κ_0 estimated in (a), showing that the conductivity of erythrocyte suspension is independent of the applied field at least up to 0.5 kV/cm. Then, a voltage pulse of desired intensity and duration was applied, and the oscilloscope traces were photographed as shown in Fig. 2. When the voltage was sufficiently high, oscilloscope 2 showed a time-dependent signal. Since a_1/a_2 had been set equal to $\kappa_0 A/d$, the signal was proportional to $\Delta\kappa$:

$$a_2I - a_1V = (a_2A/d)(\kappa - \kappa_0)V = a_2A\Delta\kappa E \qquad (2)$$

The field intensity, E, was estimated from the trace on oscilloscope 1.

(c) Changes in conductivity after the pulsation were measured by closing the

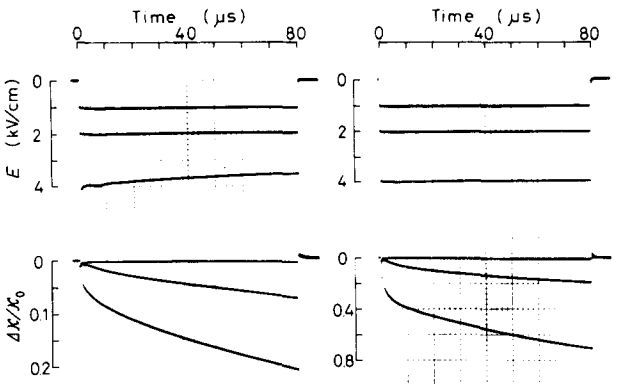

Fig. 2. Waveforms of high voltage pulses (upper graphs) and time courses of conductivity increase in erythrocyte suspensions (lower graphs). Left graphs, erythrocytes in isotonic NaCl at 19% (v/v); right graphs, in 10% NaCl/90% sucrose isotonic mixture. Type b measurements described in Materials and Methods were performed, where a_1 and a_2 were so adjusted that the vertical deflection in lower graphs roughly corresponds to $\Delta\kappa/\kappa_0$. Temperature of the samples before pulsation was 25°C.

relay in Fig. 1 after a delay of 1 ms. A sinusoidal voltage of 10 kHz was used in these measurements, and the alternating current was measured with oscilloscope 1 which in this case was connected directly to the upper-right clamp in the figure. This method covered a time range of 1 ms—10 s. (d) Slower changes were measured by transferring the pulsation cell back onto the lower clamps in Fig. 1 and recording the magnitude of the current under the sinusoidal voltage with the recorder. (e) Conductivity changes immediately after the pulsation were inferred by applying a second pulse after various intervals (see Results); $\Delta\kappa$ during the second pulse was measured in the same way as in (b).

Results

Conductivity increment during pulsation

Fig. 2 shows typical waveforms of the high voltage pulses (upper graphs) and the conductivity increments in 19% (v/v) erythrocyte suspensions during the pulsation (lower graphs); type b measurements described in Materials and Methods were performed, and the vertical scales have been converted to field intensity, E, in upper graphs and relative conductivity increment, $\Delta\kappa/\kappa_0$, in lower graphs. In isotonic NaCl, the field intensity degraded slightly with time above 2 kV/cm, as seen in the bottom trace in the upper left, because of the limited power of the Cober pulser. Top traces in the graphs show that both in isotonic NaCl and in 10% NaCl/90% sucrose isotonic mixture the conductivity remained at κ_0 as long as E did not exceed a threshold of about 1.5 kV/cm. With higher field intensities, conductivity of the erythrocyte suspension started to increase at the instant of field application. Time courses of this conductivity increase were approximately the same at high and low ionic strengths, although the magnitudes were much greater in the 10% NaCl/90% sucrose medium. At E greater than about 3 kV/cm, the time courses consisted of a rapid (approx. 1 μs) and a slow (approx. 100 μs) phases. In no cases did we observe a satura-

tion of conductivity increase. In the low ionic medium under a field of 4 kV/cm, conductivity continued to increase at least up to 1 ms; an acceleration was even observed at about 0.5 ms. The acceleration is probably due to electrophoretic leakage of intracellular ions as will be discussed later. Long pulsation in high ionic media was avoided because of the Joule heating.

Part of the conductivity increment in the isotonic NaCl suspension resulted from the Joule heating (a temperature increment of 3.4°C is expected under an 80 μs pulse at 4 kV/cm). The amount of the heat effect was estimated by the same type of measurement on a 72% NaCl/28% sucrose solution, which had approximately the same κ_0 as the erythrocyte suspension over the temperature range of 5—37°C. Conductivity of this solution increased linearly with time, the slope being proportional to E^2. The increment in the solution was assumed to represent the contribution of the heat effect to the observed $\Delta\kappa$ in the erythrocyte suspension. In the lower-left graph in Fig. 2, the middle trace coincidentally approximates this heat-dependent part of the bottom trace.

Fig. 3 summarizes the conductivity increments in the high and the low ionic erythrocyte suspensions under electric fields of various intensities. Values shown here are the net increments after the correction for the heat effect. Since conductivity increase was biphasic under high fields, as mentioned above, both $\Delta\kappa/\kappa_0$ at 2 μs and 80 μs are plotted in the figure. The threshold field intensity, E_{th}, above which the increase was detectable ($\Delta\kappa/\kappa_0 \geqslant 0.01$), was about 1.8 kV/cm at 2 μs and 1.2 kV/cm at 80 μs. These values were independent of the ionic strength and coincide with the field intensities at which the most susceptible cells in the suspension are perforated with the pores under a 2 μs pulse or an 80 μs pulse, respectively * [7]. Thus, the observed increase in conductivity appears to be due to the formation of pores through which current can penetrate the cell interior. Under fields greater than 3 kV/cm, all the cells in a sample are perforated within 1 μs (Fig. 4 in Ref. 7). The slow phase probably detects the expansion of the pores.

Effect of temperature

As mentioned in Introduction, the mechanism of the voltage-induced permeability increase in cell membranes appears to be common to many systems. In the membranes of *Valonia utricularis*, Coster and Zimmermann [12] showed that the 'breakdown potential' decreased from 1.0 V to 0.65 V as the temperature was raised from 5°C to 35°C.

Erythrocyte membranes showed a similar, but much smaller, temperature dependence. Under an 80 μs pulse, the critical transmembrane potential at which the membranes are perforated was determined to be 0.80 V at 25°C and 37°C, and 0.87 V at 5°C, but the potassium release experiments (data not shown, cf. Ref. 7). In parallel with the change in the critical transmembrane potential, curves in Fig. 3 shifted slightly downward when the temperature was lowered from 25°C to 5°C; curves for 37°C were almost indistinguishable from those for 25°C. The process of pore formation is relatively insensitive to tempera-

* It shoud be noted that E_{th} is different from $E_{1/2}$ in Ref. 7, which was defined as the field intensity at which one-half of the cells in a sample are perforated with pores.

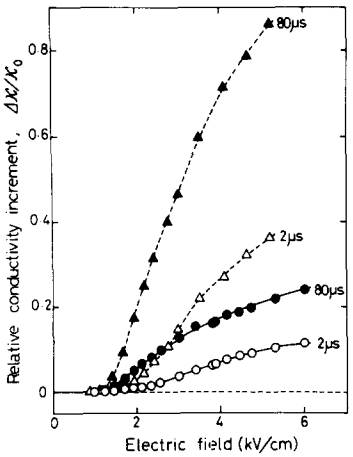

Fig. 3. Conductivity increments at different times during voltage pulsation. ○ and ●, relative conductivity increments at 2 μs and 80 μs, respectively, for erythrocytes suspended in isotonic NaCl at 19% (v/v); △ and ▲, those for erythrocytes in 10% NaCl/90% sucrose isotonic mixture at 19% (v/v). Temperature of the samples before pulsation was 25° C. That part of conductivity increment which is due to the Joule heating has been subtracted as described in text.

ture in contrast to the marked temperature dependence of the resealing process [8].

Response to linearly increasing electric field

Previous works on the voltage-induced permeability changes [1—8,12] all employed voltage pulses of very fast rise times. In order to see whether the field 'jump' is necessary for the pore formation, gradually increasing electric fields were applied to erythrocyte suspensions. Fig. 4 shows that, in both high and low ionic media, conductivity started to increase as soon as the field intensity reached the threshold of about 1.5 kV/cm irrespective of the rate of field rise. Thus, the pore-forming mechanism responds to field intensity but not its time derivatives.

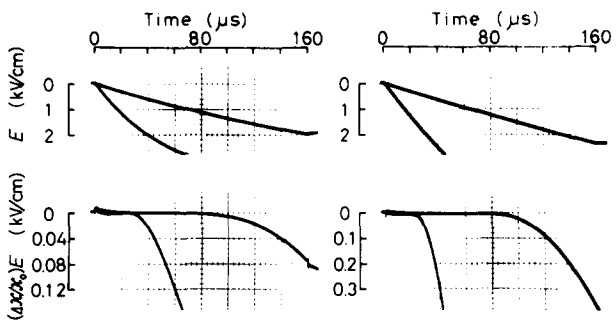

Fig. 4. Conductivity changes under linearly increasing electric field. Upper graphs, waveforms of quasi-linearly increasing field generated by the insertion of shunt capacitance (Fig. 1); lower graphs, differential signal at oscilloscope 2 in Fig. 1, which is proportional to $(\Delta\kappa/\kappa_0)E$ as shown in Eqn. 2 in text. Left graphs are for erythrocytes in isotonic NaCl at 19% (v/v); right graphs, in 10% NaCl/90% sucrose. Temperature before pulsation was 25° C.

Double-pulse experiments

In order to monitor the conductivity changes after the pulsation, a second pulse was applied after various intervals. Since the intensity of the second pulse was obligatorily the same as the first one, what we observed in these experiments was the conductivity increment due to the second pulse on top of the residual increment due to the first one.

Traces 2 in Fig. 5 show that, when the interval between the two pulses was sufficiently short, conductivity continued to increase disregarding the intermission. Again the membranes did not respond to the rapid fall and rise in field intensity. When the interval was increased to 10 ms, conductivity under the second pulse started from a value smaller than the final value under the first pulse (compare traces 1 and 2′ in Fig. 5). It appears that the increased conductivity had returned toward the original value during the long intermission.

Depencence of $\Delta\kappa/\kappa_0$ under the second pulse on the length of the intermission is summarized in Fig. 6. $\Delta\kappa/\kappa_0$ at 2 μs under the second pulse approached the corresponding value under the first pulse as the interval was increased from μs to ms. $\Delta\kappa/\kappa_0$ at the end of the second pulse, on the other hand, changed little with the interval up to ms. The apparent recovery during the intermission appears to be easily reversed by the second pulse. Conversely, the actual recovery is probably greater and faster than is suggested by the 2-μs curves; in fact, 1 μs curve for the data in Fig. 6b (not shown because of lower accuracy) decreased to 0.3 by 10^{-4} s and to less than 0.25 by 10^{-3} s.

The conductivity increments shown in Fig. 6a are not corrected for the Joule heating. Similar double-pulse experiment on the 72% NaCl/28% sucrose solution showed that the heating effect of the two pulses were additive as long as the intermission was less than 10^{-1} s, beyond which the heat generated by the first pulse started to dissipate before the second pulse. Thus the decline of the curves in Fig. 6a at about 1 s is due mainly to the cooling of the sample by thermal conduction.

Conductivity changes after pulsation

Curves S in Fig. 6 show the conductivity changes after pulsation measured under the small amplitude sinusoidal voltage. Although limited to ms or slower changes, these measurements were free from the high voltage perturbation

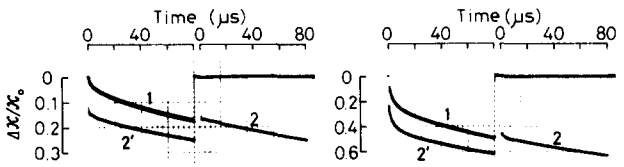

Fig. 5. Typical conductivity changes under two successive pulses. Left graph, erythrocytes at 19% (v/v) in isotonic NaCl under 3.7-kV/cm pulses; right graph, in 10% NaCl/90% sucrose isotonic mixture under 3.1-kV/cm pulses. Traces 1 and 2, response to two identical 80-μs pulses with an interval of 5 μs (single sweep triggered at the beginning of the first pulse); traces 1 and 2′, a separate experiment with an interval of 10 ms (two sweeps). Traces 1 for the two experiments overlap with each other. Temperature before pulsation was 25° C.

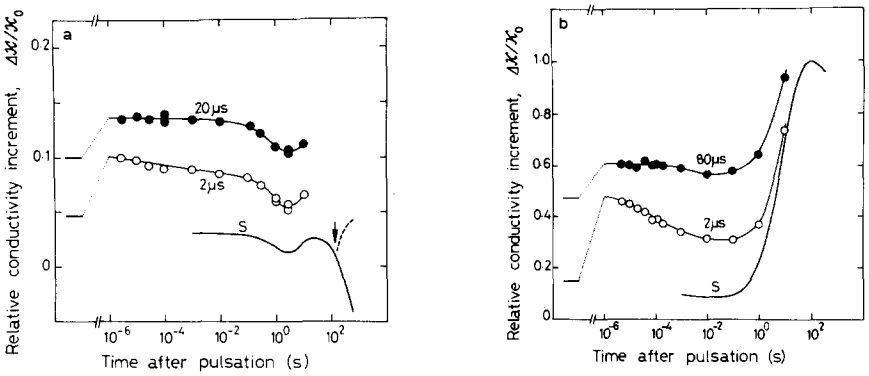

Fig. 6. Conductivity changes after pulsation. (a) Erythrocytes in isotonic NaCl at 19% (v/v) after treatment with a 20 μs pulse at 3.7 kV/cm; (b) in 10% NaCl/90% sucrose after treatment with an 80 μs pulse at 3.1 kV/cm. Conductivities in the range of 3 μs—10 s were inferred by applying a second pulse of the same intensity as the first one after various intervals (cf. Fig. 5). ○ and ●, relative conductivity increments (with reference to the untreated sample) during the second pulse while the horizontal bars at left denote the increments during the first pulse. Relatively slow changes (1 ms—10 min) were followed by type c and d measurements described in Materials and Methods and are shown in curves S. The arrow in (a) indicates an addition of 2/10 vol. of isotonic sucrose solution to the sample in the pulsation cell. This addition produced a signal shown (- - - - -) on the chart recorder that measured the total current (the ordinate scale in the figure has been converted to $\Delta\kappa/\kappa_0$ and does not apply to the dashed curve). The addition of sucrose did not alter the total current appreciably, because the decrease in conductivity was compensated by the increase in the sample volume. The slow increase that followed indicated gradual shrinkage of the cells as explained in text. Conductivity increments in this figure are not corrected for the Joule-heating effect.

involved in the double-pulse experiments. In all cases $\Delta\kappa/\kappa_0$ thus obtained at 1 ms was considerably smaller than $\Delta\kappa/\kappa_0$ at the end of the preceding pulse. Major 'recovery' takes place in the μs time range.

In Fig. 6a, the fall of curve S at about 1 s is due to the cooling as has been discussed above. The hump at about 20 s was almost absent when the suspending medium was replaced with isotonic KCl, of which the conductivity was about 25% higher than the isotonic NaCl solution. This indicates that the uprise in $\Delta\kappa/\kappa_0$ resulted from the diffusional efflux of K^+ from the perforated cells. In fact the previous study [6] has shown that the exchange of Na^+ and K^+ across the perforated membranes occurs in about a minute under these conditions. The final, and large decrease in $\Delta\kappa/\kappa_0$ in Fig. 6a is due to the colloid osmotic swelling of the perforated cells [6—8] which reduces the volume of the extracellular medium. The dashed line shows that this process could be reversed by the addition of sucrose at the arrow; shrinkage of perforated cells following the addition of sucrose has already been demonstrated in Ref. 8.

In the low ionic medium, the diffusional efflux of ions greatly increases the conductivity of the extracellular medium. Since the influx of sucrose is much slower than the efflux of intracellular ions, the cells initially shrink in sucrose media [6,7]. These two effects resulted in an almost 100% increase in the conductivity of total suspension at about 10^2 s as is seen in Fig. 6b. As sucrose entered the cells, they swelled again [6,7], and the conductivity started to decrease as is seen in the final portion of curve S.

Discussion

Factors responsible for the conductivity changes

If we approximate the shape of erythrocytes with an oblate spheroid of major and minor semi-axes a and b (Fig. 7), κ of an erythrocyte suspension can be calculated as a function of seven parameters as shown in Appendix I:

$$\kappa = \kappa(G_m, \kappa_e, \kappa_i, a, \nu, \theta_0, \Phi) \tag{3}$$

where G_m is the membrane conductance/unit area (at the equator), κ_e and κ_i the extra- and intracellular conductivities, $\nu \equiv b/a$ the axial ratio, θ_0 the angle between b and the direction of applied field (under the assumptions made in the calculation, the case of randomly oriented cells is equivalent to $\theta_0 = \pi/3$), and Φ the volume concentration of the cells.

Of these parameters, κ_e was measured to be 15.7 $m\Omega^{-1}$/cm for the isotonic NaCl and 1.58 $m\Omega^{-1}$/cm for the 10% NaCl/90% sucrose medium at 25°C, and κ_i has been estimated at 5 $m\Omega^{-1}$/cm [13]. For intact human erythrocytes, a = 4.3 μm and ν = 0.28 [7]. Since G_m of intact erythrocyte membrane is less than, and probably a few orders of magnitude smaller than, 0.1 Ω^{-1}/cm^2 [10], we have used $G_m = 0$ in the calculation of κ_0, giving κ_0 = 10.8 $m\Omega^{-1}$/cm for 19% (v/v) suspension in isotonic NaCl and κ_0 = 1.09 $m\Omega^{-1}$/cm in 10% NaCl/90% sucrose. These values compare favorably with the experimental values of κ_0 at 11.1 $m\Omega^{-1}$/cm and 1.21 $m\Omega^{-1}$/cm for the isotonic NaCl and the 10% NaCl/90% sucrose suspensions, respectively.

Possible roles of the seven parameters in the voltage-induced changes in κ of erythrocyte suspensions are discussed separately below.

(i) G_m. Except for the trivial effect of Joule heating, increase in the conducitivity of erythrocyte suspension was detected only when the field intensity exceeded the threshold that coincided with the threshold for the voltage-induced pore formation (Fig. 3). The threshold was independent of the ionic

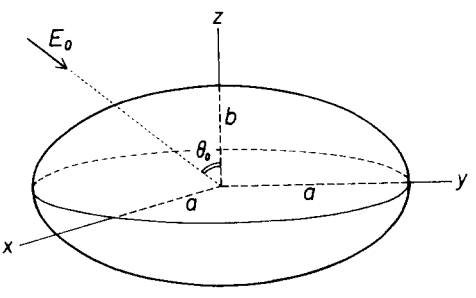

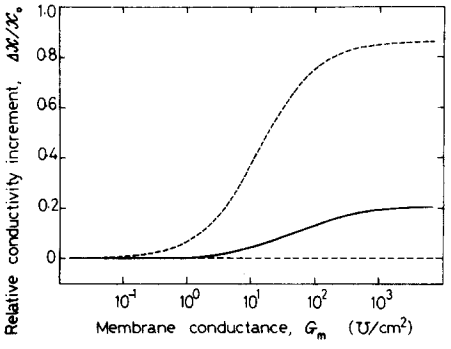

Fig. 7. A spheroidal cell with major and minor semi-axes a and b exposed to a uniform electric field E_0.

Fig. 8. Theoretical conductivities for suspension of oblate spheroidal cells. ———, cells suspended in isotonic NaCl at 25°C (extracellular conductivity, κ_e, = 15.7 $m\Omega^{-1}$/cm); - - - - - -, in 10% NaCl/90% sucrose isotonic mixture (κ_e = 1.58 $m\Omega^{-1}$/cm). Major axies, a, of the cells = 4.3 μm; axial ratio, ν, = 0.28; volume concentration, Φ, = 0.19; intracellular conductivity, κ_i, = 5.0 $m\Omega^{-1}$/cm. Orientation of the cells is assumed to be random. These curves are to be compared with the experimental results in Fig. 3.

strength and changed little with temperature both for the conductivity increase (Fig. 3) and for the perforation [7]. Under fields greater than 3 kV/cm, considerable increase in κ occurred within 1 μs (Fig. 2, the rapid phase), by which the initial perforation was complete [7]. The primary cause of the observed changes in κ of erythrocyte suspensions, therefore, appears to be an increase in G_m as the result of the perforation.

The rapid and large increase in κ during pulsation mainly reflects the voltage-induced increase in G_m, because other factors would change only slowly (κ_e, Φ) or are unlikely to induce such a large increment (a, ν, θ_0); κ_i would affect κ only after G_m becomes greater than 10 Ω^{-1}/cm^2. If we assume that the observed $\Delta\kappa/\kappa_0$ in Fig. 3 is entirely dependent on G_m, the membrane conductance during pulsation can be estimated from the theoretical curves in Fig. 8. Under a field of 4 kV/cm, for example, G_m would be approximately 10^1 Ω^{-1}/cm^2 at 2 μs and 10^2 Ω^{-1}/cm^2 at 80 μs both in the high and in the low ionic media. Isotonic saline in a layer of the same thickness as the cell membrane (approx. 10 nm) has a conductance/unit area in the order of 10^4 Ω^{-1}/cm^2. Therefore, the above G_m would correspond to openings of 0.1—1% of the membrane area. After the field is removed, G_m probably returns to much less than 10^0 Ω^{-1}/cm^2 as will be discussed below.

(ii) κ_e. Conductivity of the NaCl/sucrose solutions was independent of the applied field at least up to 6 kV/cm, except for the heat effect. Any change in κ_e, therefore, must be the result of the perforation that allows the leakage of ions through the membranes. The leakage by diffusion takes at least 10^{-1} s, because the diffusion constant of small ions in water is in the order of 10^{-5} cm^2/s [14] and the dimension of an erythrocyte as well as the separation between the cells in the 19% (v/v) suspension are in the order of 10 μm. This low process was observed as the uprise in κ in Fig. 6. Under intense electric fields, on the other hand, ions will move electrophoretically; the speed under a field of 4 kV/cm will be about 2 cm/s, or 10 μm/0.5 ms, for small ions of which the mobility in water ranges around $5 \cdot 10^{-4}$ cm^2/V per s [15]. Therefore, the acceleration of conductivity increase during long pulsation mentioned under Fig. 2 is likely the reflection of increasing κ_e due to the electrophoretic leakage of ions.

(iii) κ_i. Comparison of Figs. 3 and 8 suggests that under a long, intense field $\Delta\kappa/\kappa_0$ would exceed the theoretical maximum of 0.21 for the isotonic NaCl and 0.86 for the 10% NaCl/90% sucrose suspension. Thus, part of the observed $\Delta\kappa/\kappa_0$ should be attributed to factors other than G_m.

In the theoretical κ shown in Fig. 8, κ_i is taken as 5 $m\Omega^{-1}/cm$ according to the experimental determination by Pauly and Schwan [13]. These authors also showed that theoretical κ_i calculated from the ionic content of erythrocytes was twice the observed value; they suggested that the discrepancy may be explained by hydrodynamic and electrostatic interactions of the ions and hemoglobin. Possible liberation of the ions under intense electric fields would explain the rather large $\Delta\kappa/\kappa_0$ in Fig. 3, because theoretical $\Delta\kappa/\kappa_0$ for κ_i = 10 $m\Omega^{-1}/cm$ is approximately 50% higher than that in Fig. 8 in the region where $G_m > 10^2$ Ω^{-1}/cm^2. Value of κ_i does not affect κ unless $G_m \geqslant 10$ Ω^{-1}/cm^2. Therefore, post-pulse changes in κ are not related with κ_i.

(iv) a, ν, θ_0. A theoretical calculation (Kinosita, K., Jr., unpublished results)

has shown that oblate cells under an intense electric field elongate in the direction of the field and at the same time rotate so that their major axis becomes parallel with the field. Both processes may occur in the submillisecond range under a field of a few kV/cm. These geometrical changes would increase κ (e.g. compare rows 1 and 2, 3 and 4, or 5 and 2 in Table I), and could account for part of the large $\Delta\kappa/\kappa_0$ during pulsation. The rapid optical signals under electric fields observed by Tsong and Kingsley [4] may well correspond to the change in geometry.

In order to investigate this possibility, three samples corresponding to rows 1, 5, and 6 in Table I were prepared. The sample for row 1 (control) was 19% (v/v) suspension of normal erythrocytes in the isotonic NaCl. Sphering under constant cell volume (row 5) was achieved by the addition of 1 mM of 1-anilino-8-napthalene sulfonate (ANS) [16]. Swollen spherical erythrocytes (row 6) were prepared by replacing the medium with (0.57 × isotonic) NaCl, of which κ_e was 9.30 $m\Omega^{-1}$/cm. κ_0 of these samples were 11.3 $m\Omega^{-1}$/cm, 12.2 $m\Omega^{-1}$/cm, and 5.8 $m\Omega^{-1}$/cm, respectively, in reasonable agreement with the theoretical prediction in Table I. Then the samples were exposed to a 3.7 kV/cm pulse and the conductivity increment was determined by the type b measurement. κ/κ_0 at 2 μs was 1.05 for control, 1.06 in the presence of ANS, and 1.14 for the hypotonic suspension. Comparison of these velues with Table I indicates that in all three samples G_m became approx. 10 Ω^{-1}/cm^2 at 2 μs. Sphering did not affect the rapid phase. On the other hand, change in the slow phase was considerably reduced upon sphering: κ/κ_0 at 80 μs was 1.15 for control, 1.10 in the presence of ANS, and 1.27 for the swollen cells. Whereas the control value corresponds to a G_m greater than 10^2 Ω^{-1}/cm^2, κ/κ_0 for spherical cells would give a G_m less than 10^2 Ω^{-1}/cm^2 (Table I). This result is likely an indication that part of the slow increase in κ/κ_0 of control resulted from the reorientation effect, which is absent in spherical cells.

The magnitude of the geometrical contribution to $\Delta\kappa/\kappa_0$, however, cannot be very large as seen in Table I. This is also suggested by the absence of detectable $\Delta\kappa/\kappa_0$ below the threshold intensity. (This absence does not exclude the possibility of the geometrical changes, because the electrostatic forces involved would be proportional to the square of the field intensity.) The magnitude is probably about the size of $\Delta\kappa/\kappa_0$ at 1 ms in Fig. 6 (curves S); $\Delta\kappa/\kappa_0$ at this stages is most easily explained by altered geometry remaining after pulsation.

(v) Φ. Change in cell volume must be accompanied by permeation of water through the cell membrane. Thus, significant change in Φ is unlikely to occur in the μs range. After pulsation, gradual permeation of solutes across the perforated membrane tends to impair the osmotic balance, which is continuously restored by the efflux or influx of water. This osmotically induced change in Φ is responsible for the slowest change in κ seen in Fig. 6. Note that the rising portion in curve S in Fig. 6b follows parallel changes in κ_e and Φ, both resulting from the efflux of intracellular ions.

Number of pores/cell

The uprise in $\Delta\kappa/\kappa_0$ at about 10 s in Fig. 6a is presumed to reflect the efflux of K^+ from the perforated erythrocytes. Then, this rate constant of about 10^{-1} s^{-1} multiplied by the cell volume of $1 \cdot 10^{-10}$ cm^3 [17] gives the propor-

TABLE I

THEORETICAL CONDUCTIVITIES FOR SUSPENSIONS OF OBLATE SPHEROIDAL CELLS

1, disk-shaped cells oriented randomly in isotonic NaCl; 2, disk-shaped cells in isotonic NaCl with major axis oriented parallel with the applied field (κ_0 in relative conductivities taken as 10.8 $m\Omega^{-1}/cm$); 3, disk-shaped cells oriented randomly in 10% NaCl/90% sucrose isotonic mixture; 4, cells in 3 oriented along the field (κ_0 taken as 1.09 $m\Omega^{-1}/cm$); 5, spherical cells with the same volume as 1 in isotonic NaCl; 6, swollen, spherical cells in [0.57 × isotonic] NaCl. In all cases the intracellular conductivity, κ_i, was taken as 5.0 $m\Omega^{-1}/cm$.

		Major axis a (μm)	Axial ratio ν	Cell volume $(4/3)\pi a^3\nu$ (μm^3)	Volume concentration ϕ	Conductivity of external medium κ_e ($m\Omega^{-1}/cm$)	Conductivity of suspension, κ (relative conductivity, κ/κ_0) Membrane conductance (G_m) ($m\Omega^{-1}/cm$)			
							0	10	10^2	10^3
1	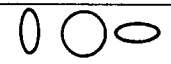	4.3	0.28	93	0.19	15.7	10.8 (1.00)	11.3 (1.04)	12.2 (1.13)	12.9 (1.20)
2		4.3	0.28	93	0.19	15.7	12.4 (1.15)	12.9 (1.20)	13.4 (1.24)	13.5 (1.25)
3		4.3	0.28	93	0.19	1.58	1.09 (1.00)	1.49 (1.37)	1.91 (1.75)	2.01 (1.85)
4		4.3	0.28	93	0.19	1.58	1.25 (1.15)	1.71 (1.57)	2.05 (1.88)	2.11 (1.94)
5		2.8	1.00	92	0.19	15.7	11.6 (1.00)	12.2 (1.05)	13.0 (1.13)	13.2 (1.14)
6		3.2	1.00	137	0.28	9.30	5.86 (1.00)	6.75 (1.15)	7.70 (1.31)	7.91 (1.35)

tionality constant between the flux j/cell and the concentration difference ΔC across the membrane:

$$j = (10^{-11}\ \mathrm{cm^3/s})\Delta C \tag{4}$$

On the other hand, the effective radius of the voltage-induced pores in the above cells is about 0.45 nm [8]. If we approximate these pores with straight cylindrical holes with radius of 0.45 nm and length of 10 nm, the thickness of the membrane, the flux/pore, j_p, will be, under the simplest assumptions, given by

$$\begin{aligned} j_p &= \pi(4.5 \cdot 10^{-8}\ \mathrm{cm})^2(1 \cdot 10^{-6}\ \mathrm{cm})^{-1} D\Delta C \\ &= (1.3 \cdot 10^{-13}\ \mathrm{cm^3/s})\Delta C \end{aligned} \tag{5}$$

where D is the diffusion constant of K^+ and is about $2 \cdot 10^{-5}\ \mathrm{cm^2/s}$ at 25°C [14]. Taking the ratio of Eqns. 4 and 5, we obtain the number of pores/cell, n_p, as

$$n_p = j/j_p \approx 10^2 \tag{6}$$

This is probably an underestimate, because we have neglected the friction at the pore wall and other complicating factors in the calculation of j_p.

Appendix II provides another means of estimating n_p, from G_m and the single pore conductance σ_p. The cylindrical pore above filled with isotonic KCl, of which the conductivity is about 20 $\mathrm{m\Omega^{-1}/cm}$ [15], will have a conductance given by

$$\sigma_p = \pi(4.5 \cdot 10^{-8}\ \mathrm{cm})^2(1 \cdot 10^{-6}\ \mathrm{cm})^{-1}(2 \cdot 10^{-2}\ \Omega^{-1}/\mathrm{cm}) = 1.3 \cdot 10^{-10}\ \Omega^{-1} \tag{7}$$

On the other hand, $\Delta\kappa/\kappa_0$ of the corresponding erythrocyte suspension was 0.016 at 1 ms (Fig. 6a) after the correction for the heat effect. If we assume that this $\Delta\kappa/\kappa_0$ is entirely dependent on G_m, G_m would be estimated at $2.5\ \Omega^{-1}/\mathrm{cm^2}$ from Fig. 8. From these σ_p and G_m, n_p is calculated as (see Eqn. 28A in Appendix II)

$$\begin{aligned} n_p &= (4\pi/3)(4.3 \cdot 10^{-4}\ \mathrm{cm})(1.2 \cdot 10^{-4}\ \mathrm{cm})(2.5\ \Omega^{-1}/\mathrm{cm^2})(1.3 \cdot 10^{-10}\ \Omega^{-1})^{-1} \\ &= 4 \cdot 10^3 \end{aligned} \tag{8}$$

This number is more than an order of magnitude greater than the previous estimate in Eqn. 6. The discrepancy suggests that actual G_m is much smaller than $2.5\ \Omega^{-1}/\mathrm{cm^2}$ and that $\Delta\kappa/\kappa_0$ at 1 ms is contributed by other factors as already discussed above (note that the neglection of the friction, etc. is common to both estimates).

The difference of several orders of magnitude between G_m during and after the pulsation remains to be explained. The pores may well be decorated with charged residues as has been suggested previously [7]. These charges and the probable irregularities in the structure of the pores will act as energy barriers against the passage of ions as long as the driving force is weak. The barriers, however, could be overcome by the ions driven by the intense electric field generated by the voltage pulsation (a transmembrane potential of 1 V corresponds to an electric field of 10^6 V/cm in the membrane), or the barriers them-

selves might be swung out of the way by the electric field. Thus the membrane conductance under large transmembrane potentials could be much greater than is expected from the diffusional permeability or the conductance under small voltage.

Appendix I

Conductivity of a suspension of spheroidal cells

First we calculate the potential profile around a single cell placed in a uniform electric field. The case of non-conducting cell membrane has already been treated in the previous paper [7].

As is shown in Fig. 7, we consider an oblate spheroidal cell with membrane of negligible thickness at the origin exposed to a uniform electric field E_0 lying in the x-z plane. We introduce the oblate spheroidal coordinates (u, v, φ) such that

$$(x^2 + y^2)^{1/2} = h(u^2 + 1)^{1/2}(1 - v^2)^{1/2}$$

$$z = huv$$

$$\tan^{-1}(y/x) = \varphi \tag{1A}$$

$$h = a(1 - v^2)^{1/2}$$

where $\nu \equiv b/a$ is the axial ratio of the cell. The surface of the cell is represented by

$$u = a\nu/h \equiv c \tag{2A}$$

We assume, for the sake of mathematical simplicity, that the membrane conductance/unit area g_m is given by

$$g_m = G_m/[1 + v^2(1 - \nu^2)/\nu^2]^{1/2} \tag{3A}$$

That is, the conductance at the equator is G_m and that at the poles is νG_m. This assumption is equivalent to the limit of infinitely thin membrane of uniform conductivity enclosed by a pair of confocal surfaces.

In the steady state, the electric potentials in the extra- and intracellular spaces, V_e and V_i, satisfy Laplace's equation:

$$\nabla^2 V_e = \nabla^2 V_i = 0 \tag{4A}$$

At the cell surface the normal component of the current density must be continuous:

$$\kappa_e[\partial V_e/\partial u]_{u=c} = \kappa_i[\partial V_i/\partial u]_{u=c} \tag{5A}$$

where κ_e and κ_i are the conductivities of the extra- and intracellular media. Ohm's law applied to the membrane together with the continuity states

$$\kappa_i[\partial V_i/\partial u]_{u=c} = g_m[V_e - V_i]_{u=c} \tag{6A}$$

Finally, V_e at large distances ($u \to \infty$) must take the form

$$V_e(u, v, \varphi)_{u\to\infty} = E_0(z \cos\theta_0 + x \sin\theta_0)$$
$$= E_0 h[uv \cos\theta_0 + (u^2+1)^{1/2}(1-V^2)^{1/2} \cos\varphi \sin\theta_0] \quad (7A)$$

where θ_0 is the angle between E_0 and the z-axis.

Solving Eqns. 4A under the boundary conditions of Eqns. 5A—7A, we obtain

$$V_e = E_0 h[uv \cos\theta_0 + (u^2+1)^{1/2}(1-v^2)^{1/2} \cos\varphi \sin\theta_0]$$
$$- E_0 hP[(3v/2)/(1-v^2)^{3/2}][u \tan^{-1}(1/u) - 1]\, v \cos\theta_0$$
$$+ E_0 hQ[(3v/4)/(1-v^2)^{3/2}][(u^2+1)^{1/2} \tan^{-1}(1/u) - u/(u^2+1)^{1/2}](1-v^2)^{1/2}$$
$$\cos\varphi \sin\theta_0$$

$$V_i = E_0 h(3P/2)[\kappa_e G_m/(\kappa_e G_m - \kappa_i G_m + \kappa_e\kappa_i/av^2]\, uv \cos\theta_0 \quad (8A)$$
$$+ E_0 h(3Q/2)[\kappa_e G_m/(\kappa_e G_m - \kappa_i G_m + \kappa_e\kappa_i/a)](u^2+1)^{1/2}(1-v^2)^{1/2} \cos\varphi \sin\theta_0$$

where

$$P = \gamma_p[\kappa_e G_m - \kappa_i G_m + \kappa_e\kappa_i/av^2]/[\kappa_e G_m + (3\gamma_p/2 - 1)\kappa_i G_m + \kappa_e\kappa_i/av^2]$$
$$Q = \gamma_q[\kappa_e G_m - \kappa_i G_m + \kappa_e\kappa_i/a]/[\kappa_e G_m + (3\gamma_q/2 - 1)\kappa_i G_m + \kappa_e\kappa_i/a] \quad (9A)$$

and

$$\gamma_p = (2/3v)(1-v^2)^{3/2}/[\cos^{-1} v - v(1-v^2)^{1/2}]$$
$$\gamma_q = -(4/3v)(1-v^2)^{3/2}/[\cos^{-1} v - (2-v^2)(1-v^2)^{1/2}/v] \quad (10A)$$

For non-conducting membrane ($G_m = 0$), $P = \gamma_p$, $Q = \gamma_q$, and V_e reduces to the previous result [7]. The transmembrane potential is calculated as $\Delta V \equiv V_e - V_i$, and its maximal value ΔV_{max} is obtained as

$$\Delta V_{max} = (3/2)E_0 a\{[P \cos\theta_0(\kappa_e\kappa_i/av)/(\kappa_e G_m - \kappa_i G_m + \kappa_e\kappa_i/av^2)]^2$$
$$+ [Q \sin\theta_0(\kappa_e\kappa_i/a)/(\kappa_e G_m - \kappa_i G_m + \kappa_e\kappa_i/a)]^2\}^{1/2} \quad (11A)$$

Now we calculate the conductivity of a suspension of the cells following the method of Maxwell [18]. For $u \to \infty$, V_e in Eqn. 8A takes an asymptotic form

$$V_e = E_0 r(\cos\theta \cos\theta_0 + \sin\theta \cos\varphi \sin\theta_0)$$
$$+ E_0(P/2)(a^2 b/r^2) \cos\theta \cos\theta_0 + E_0(Q/2)(a^2 b/r^2) \sin\theta \cos\varphi \sin\theta_0 \quad (12A)$$

where (r, θ, φ) are the spherical coordinates. Therefore, if there are N cells in a sphere of radius R, and if N is not so large that we can neglect the interaction between the cells, the potential at great distances from the sphere will be

$$V_e = E_0 r \cos\omega + E_0(X/2)(Na^2 b/r^2) \cos\omega \quad (13A)$$

where ω is the angle between E_0 and the direction vector, and

$X = (P + 2Q)/3$ when the orientation of the cells is random

$X = P$ when all the cells are so oriented that $b \parallel E_0$ (14A)

$X = Q$ when all the cells are so oriented that $a \parallel E_0$

On the other hand, the potential outside a sphere of uniform conductivity κ and of radius R immersed in the medium of conductivity κ_e is given by

$$V_e = E_0 r \cos \omega + E_0 [(\kappa_e - \kappa)/(2\kappa_e + \kappa)](R^3/r^2) \cos \omega \quad (15A)$$

Equating Eqns. 13A and 15A, we obtain

$$\kappa/\kappa_e = (1 - \Phi X)/(1 + \Phi X/2) \quad (16A)$$

where $\Phi \equiv Na^2b/R^3$ is the volume concentration of the cells. Eqn. 16A gives the conductivity of the cell suspension, κ, as a function of G_m, κ_e, κ_i, a, ν, Φ, and the orientation of the cells. For the case of spherical cells ($\nu = 1$), Eqn. 16A becomes

$$\frac{\kappa}{\kappa_e} = \frac{(1 + 2\Phi)/\kappa_e + 2(1 - \Phi)[(1/\kappa_i) + (1/G_m a)]}{(1 - \Phi)/\kappa_e + (2 + \Phi)[(1/\kappa_i) + (1/G_m a)]} \quad (17A)$$

which is identical with Cole's equation [19].

Appendix II

Relation between G_m and pore conductance

Equations in Appendix I provide a means of estimating G_m, the membrane conductance/unit area (at the equator), from experimental κ/κ_e. For the electrically perforated cells, G_m thus obtained should be understood as an averaged quantity because the pores are probably formed within localized regions of the cell membrane, i.e. those regions that oppose the electrodes [7]. In the following we relate G_m with σ_p, the conductance of a single pore, and n_p, the number of the pores/cell, taking the localization of the pores into account. Only the case of spherical cells is treated below in order to avoid long equations.

Consider a spherical cell with infinitely thin membrane located at the origin and exposed to a uniform electric field E_0 of direction in $-z$ (Fig. 9). We assume that the cell is perforated within very small regions around the poles A_1 and A_2, the conductance of each perforated region being given by $n_p\sigma_p/2$. If $n_p\sigma_p/2$ is not so large that the transmembrane potential at the poles is not much different from $(3/2)E_0a$, the value for non-conducting membrane [7], the current J that flows through each perforated region is given by

$$J = (n_p\sigma_p/2)(3E_0a/2) \quad (18A)$$

The current determines the form of the extracellular potential V_e near the poles (see Ref. 20 where the solution for the intracellular potential V_i is given):

$$V_e = -J/2\pi\kappa_e r_1 \text{ (near } A_1), \quad V_e = J/2\pi\kappa_e r_2 \text{ (near } A_2) \quad (19A)$$

where r_1 and r_2 are the distances from A_1 and A_2, respectively (see Fig. 9). Elsewhere on the surface of the cell ($r = a$), V_e must satisfy

$$\partial V_e/\partial r = 0 \quad (20A)$$

At long distances from the origin, on the other hand, V_e must have the

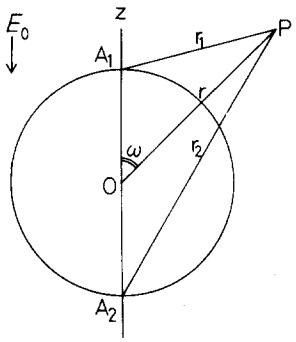

Fig. 9. A spheroidal cell of radius a at the origin O exposed to a uniform electric field E_0. The cell is perforated at the two poles A_1 and A_2. P denotes a point in the extracellular medium.

asymptotic form

$$V_e = E_0 r \cos \omega \tag{21A}$$

Solving Laplace's equation under the above boundary conditions, we obtain

$$V_e = E_0 r \cos \omega(1 + a^3/2r^3) - (J/2\pi\kappa_e)[(1/r_1) - (1/r_2) + (\psi/2a)] \tag{22A}$$

where

$$\psi = \sin h^{-1}[(a + r \cos \omega)/r \sin \omega] - \sin h^{-1}[(a - r \cos \omega)/r \sin \omega] - 2 \sin h^{-1} \cot \omega \tag{23A}$$

For sufficiently large r, the potential V_e in Eqn. 22A is approximated by

$$V_e = E_0 r \cos \omega + E_0[(1/2) - (9n_p\sigma_p/16\pi\kappa_e a)](a^3/r^2) \cos \omega \tag{24A}$$

where we have substituted Eqn. 18A for J. Since Eqn. 24A has the same form as Eqn. 15A, the conductivity, κ, of a suspension of the perforated spherical cells is again given by Eqn. 16A, where X for this case is given by

$$X = 1 - 9n_p\sigma_p/8\pi\kappa_e a \tag{25A}$$

On the other hand, Eqn. 14A becomes, for the case of spherical cells and for relatively small G_m,

$$X = 1 - 3G_m a/2\pi_e \tag{26A}$$

Equating Eqns. 25A and 26A, we obtain

$$n_p\sigma_p = 4\pi a^2 G_m/3 \tag{27A}$$

A more elaborate calculation under similar assumptions has shown that for oblate spheroidal cells Eqn. 27A becomes

$$n_p\sigma_p = 4\pi abG_m/3 \tag{28A}$$

The numerator, $4\pi abG_m$, is equal to g_m in Eqn. 3A integrated over the cell surface. The appearance of the factor 1/3 in Eqn. 28A is due to the localization of the membrane conductance as opposed to the quasi-uniformly distributed conductance in Eqn. 3A.

Acknowledgements

We thank Ray L. Nunnally and Joseph W. Schaffer for helpful suggestions about the design of the experiments. This work was supported by the United States Public Health Service Grant HL18048.

References

1 Sale, A.J.H. and Hamilton, W.A. (1968) Biochim. Biophys. Acta 163, 37—43
2 Neumann, E. and Rosenheck, K. (1972) J. Membrane Biol. 10, 279—290
3 Riemann, F., Zimmermann, U. and Pilwat, G. (1975) Biochim. Biophys. Acta 394, 449—462
4 Tsong, T.Y. and Kingsley, E. (1975) J. Biol. Chem. 250, 786—789
5 Tsong, T.Y., Tsong, T.T., Kingsley, E. and Siliciano, R. (1976) Biophys. J. 16, 1091—1104
6 Kinosita, K., Jr. and Tsong, T.Y. (1977) Proc. Natl. Acad. Sci. U.S. 74, 1923—1927
7 Kinosita, K., Jr. and Tsong, T.Y. (1977) Biochim. Biophys. Acta 471, 227—242
8 Kinosita, K., Jr. and Tsong, T.Y. (1977) Nature 268, 438—441
9 Kinosita, K., Jr. and Tsong, T.Y. (1978) Nature 272, 258—260
10 Lassen, U.V. (1972) Oxygen Affinity and Red Cell Acid Base Status (Rorth, M. and Astrup, P., eds.), pp. 291—306, Munksgaard, Copenhagen
11 Feltham, A.M. and Spiro, M. (1971) Chem. Rev. 71, 177—193
12 Coster, H.G.L. and Zimmermann, U. (1975) Biochim. Biophys. Acta 382, 410—418
13 Pauly, H. and Schwan, H.P. (1966) Biophys. J. 6, 621—639
14 Bruins, H.R. (1929) International Critical Tables (Washburn, E.W., ed.), Vol. V, pp. 63—76, McGraw-Hill, New York
15 Hamer, W.J. and Wood, R.E. (1967) Handbook of Physics (Condon, E.U. and Odishaw, H., eds.), Chap. 9, McGraw-Hill, New York
16 Yoshida, S. and Ikegami, A. (1974) Biochim. Biophys. Acta 367, 39—46
17 Whittam, R. (1964) Transport and Diffusion in Red Blood Cells, Edward Arnold, London
18 Maxwell, J.C. (1873) A Treatise on Electricity and Magnetism, Art. 314, Clarendon, Oxford
19 Cole, K.S. (1937) Trans. Faraday Soc. 33, 966—972
20 Landau, L.D. and Lifshits, E.M. (1960) Electrodynamics of Continuous Media, Chap. III. Pergamon, Oxford